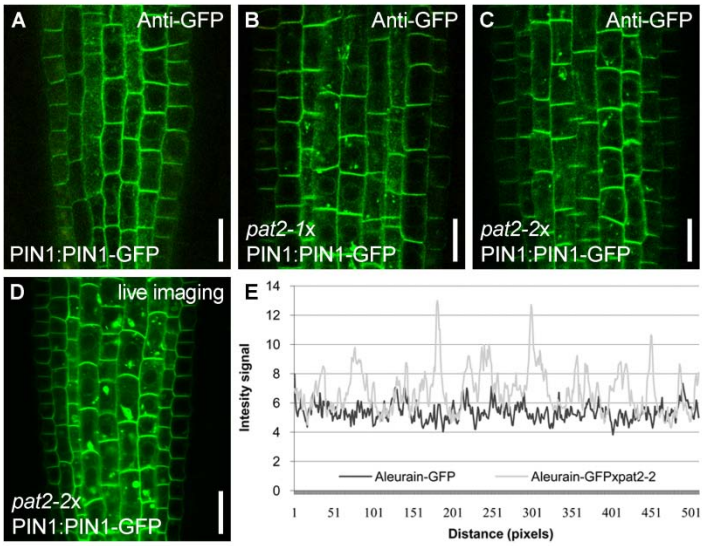

Supplemental Figure 1. *pat2* displays intracellular accumulation of PM and soluble proteins.

(A) to (D) PIN1-GFP accumulates intracellularly in *pat2-1* and *pat2-2* mutants. Immunolocalization using anti-GFP antibodies shows PIN1-GFP localization in the stele cells of control (A), *pat2-1* (B) and *pat2-2* (C). Live imaging showing PIN1-GFP agglomerations in the stele cells of *pat2-2* mutant (D).

(E) The intensity of Aleurain-GFP signal plotted on a distance of about 500 pixels shows weaker Aleurain-GFP accumulation in the wild-type meristematic zone (dark grey) while, in the *pat2-2* mutant, the Aleurain-GFP signal shows higher accumulation (light gray). The higher intensity of Aleurain-GFP signal shows the abnormal accumulation of this protein in the *pat2* mutant (n = 36). Scale bars are 20 μm.

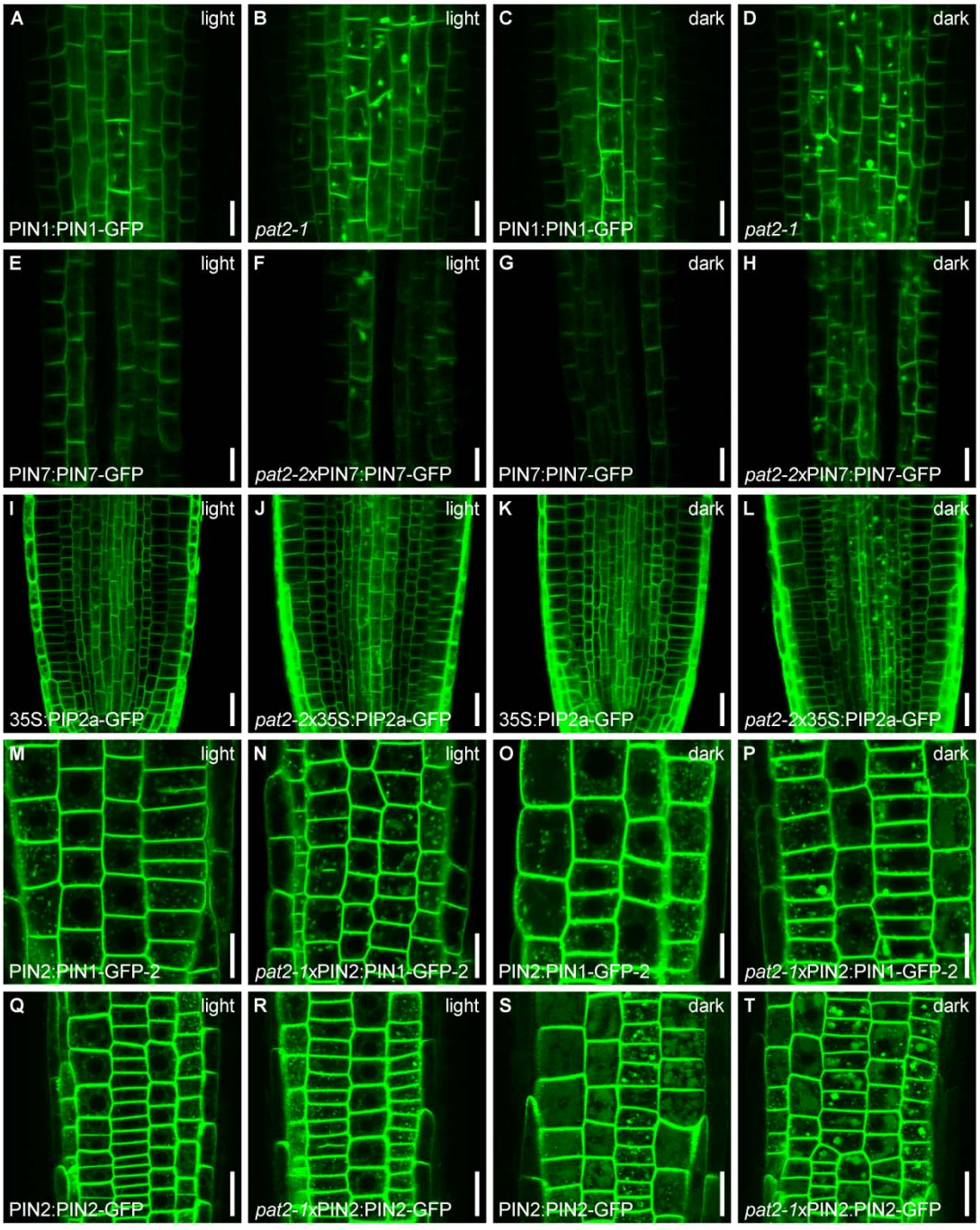

Supplemental Figure 2. *pat2* mutation causes enhanced vacuolar accumulation of polar and nonpolar integral PM proteins.

(A) to (L) PM proteins such as PIN1-GFP, PIN7-GFP and PIP2a-GFP display strong accumulation in the stele cells of *pat2* mutants ([B], [F] and [J]), as compared to the control ([A], [E] and [I]). The dark treatment enhances the accumulation of PIN1-GFP (4 h dark treatment),

PIN7-GFP (2 h dark treatment) and PIP2a-GFP (2.5 h dark treatment) in the *pat2* mutants ([D], [H] and [L]), as compared to the control ([C], [G] and [K]).

(M) to (T) PM markers expressed in the epidermal and cortical cells of the root show intracellular agglomeration in the *pat2* mutant. Both, PIN1-GFP-2 and PIN2-GFP display in light weak accumulation in the *pat2* mutant ([N] and [R]), as compared to the controls ([M] and [Q]). The dark treatment (2.5 h) causes enhancement of PIN1-GFP-2 and PIN2-GFP agglomerations in *pat2-1* ([P] and [T]), as compared to the control ([O] and [S]).

Scale bars are 10 μm (A) to (H) and 20 μm (I) to (T).

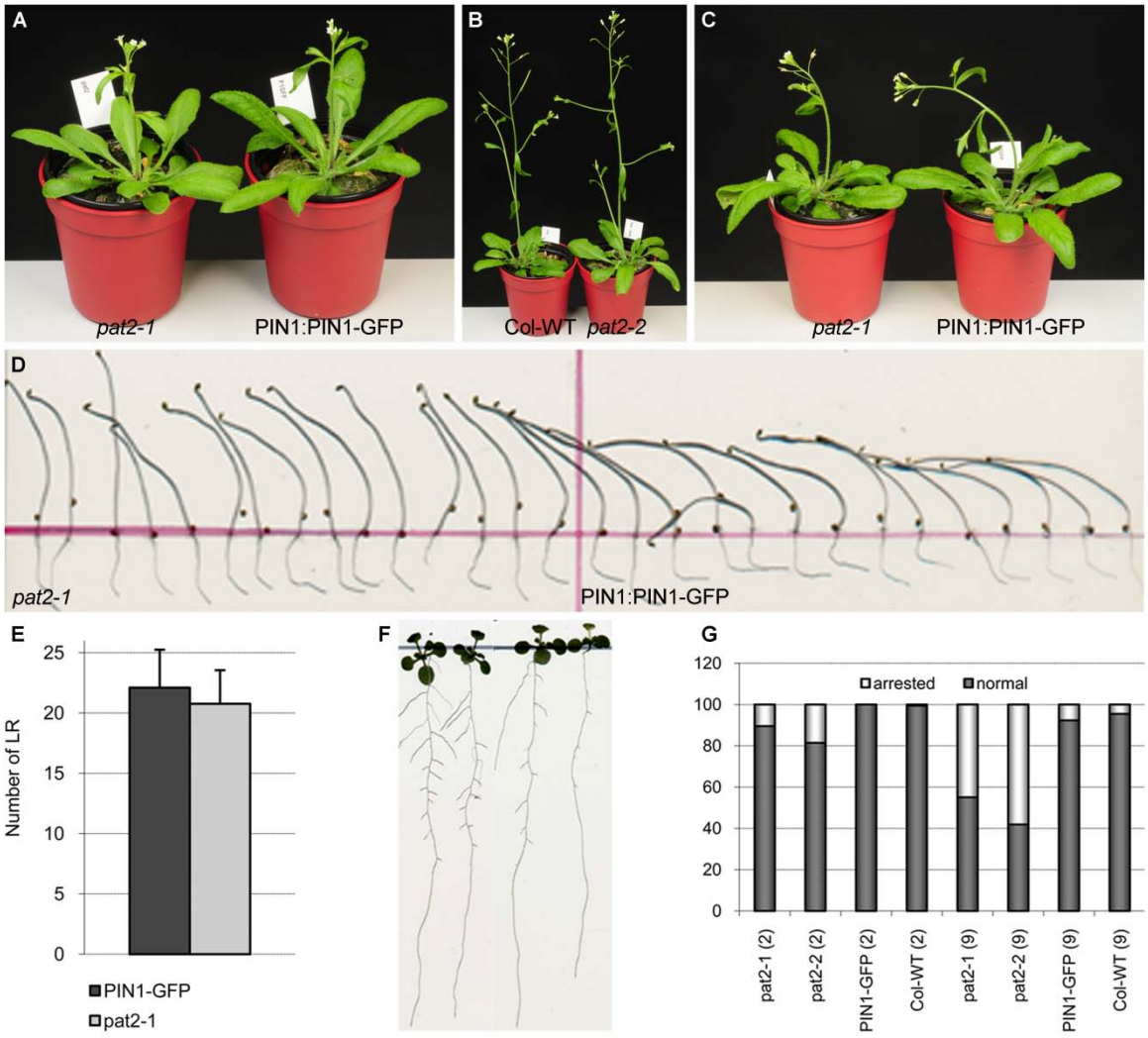

Supplemental Figure 3. *pat2* morphological phenotypes remind of mutants defective in vacuolar function.

(A) and (B) Adult plants of *pat2-1* (left) (A) and *pat2-2* (right) (B) show similar morphological phenotypes as $PIN1_{pro}$*:PIN1-GFP* (right) (A) and wild-type (left) (B).

(C) The shoot gravitropic response of 90^{o} gravistimulated plants is reduced in *pat2-1* mutant (left) comparing with the control (right).

(D) The hypocotyl gravitropic response is reduced in *pat2-1* seedlings (left) comparing with the control (right).

(E) The number of emerged lateral roots by the *pat2-1* grown on standard Arabidopsis medium is not much affected (n = 75).

(F) The non-arrested *pat2-2* seedlings (right) on medium without sucrose form less lateral roots comparing with the wild-type (left).

(G) *pat2* mutants grown on medium without sucrose display arrested phenotype. The histogram shows the percentage of normal and arrested seedlings. The arrested percentage is much higher when the mutant lines are older (2, 2-month-old seeds; 9, 9-month-old seeds; n = 111 *PIN1*$_{pro}$*:PIN1-GFP*, 239 *pat2-2*, 181 wild-type, 210 *pat2-2* seedlings for 2-month-old seeds and 247 *PIN1*$_{pro}$*:PIN1-GFP*, 167 *pat2-2*, 198 wild-type and 215 *pat2-2* seedlings for 9-month-old seeds).

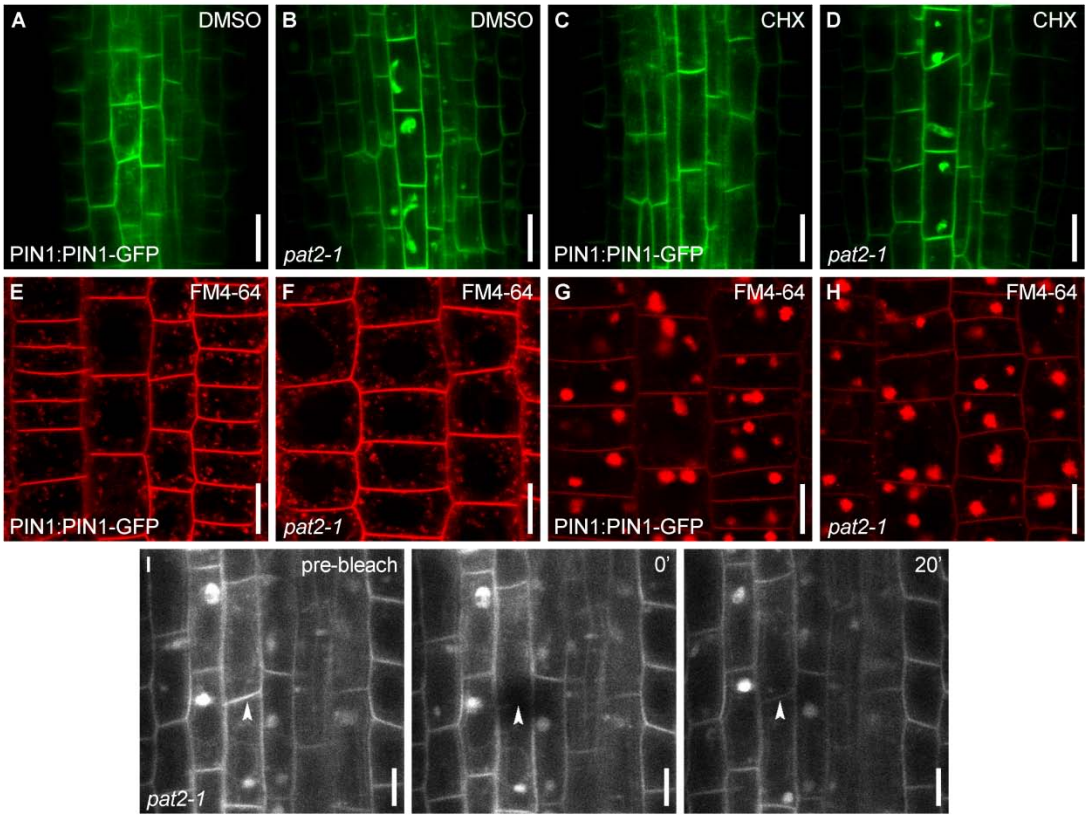

Supplemental Figure 4. PIN1-GFP trafficking to PM, recycling and early endocytosis are not affected in *pat2*.

(A) to (D) The polar localization and abundance of PIN1-GFP at the basal PM is shown in wild-type (A) and *pat2-1* (B) stele cells treated with DMSO and wild-type (C) and *pat2-1* (D) treated with protein biosynthesis inhibitor, cycloheximide (CHX; 50 µM) for 3.5 h.

(E) and (F) FM4-64 (4 µM) uptake within 25 minutes is shown in $PIN1_{pro}$*:PIN1-GFP* (E) and *pat2-1* (F) epidermal cells.

(G) and (H) FM4-64 (4 µM) agglomeration in the BFA compartment is shown in $PIN1_{pro}$*:PIN1-GFP* (G) and *pat2-1* (H) treated 1 h with BFA 50 µM.

(I) Fluorescent Recovery After Photobleaching (FRAP) of PIN1-GFP before bleaching, 0 minutes and 20 minutes after bleaching is shown in *pat2-1* mutant. Note the recovery of PIN1-GFP at the bleached PM.

Scale bars are 10 µm (A) to (H) and 5 µm (I).

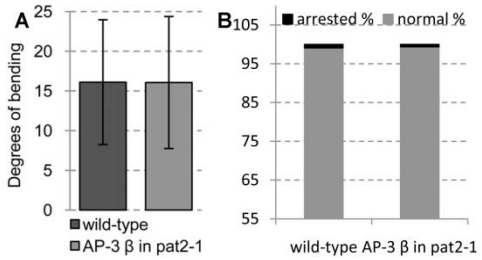

Supplemental Figure 5. *AP-3 β_{pro}:AP-3 β-GFP* complements *pat2-1* defects.

(A) and (B) *AP-3 β_{pro}:AP-3 β-GFP* complements the hypocotyls defective response (n = 109) (A) and the arrested phenotype (n = 337 wild-type; n = 329 *AP-3 β_{pro}:AP-3 β-GFP* in *pat2-1*) (B) of *pat2-1* mutant.

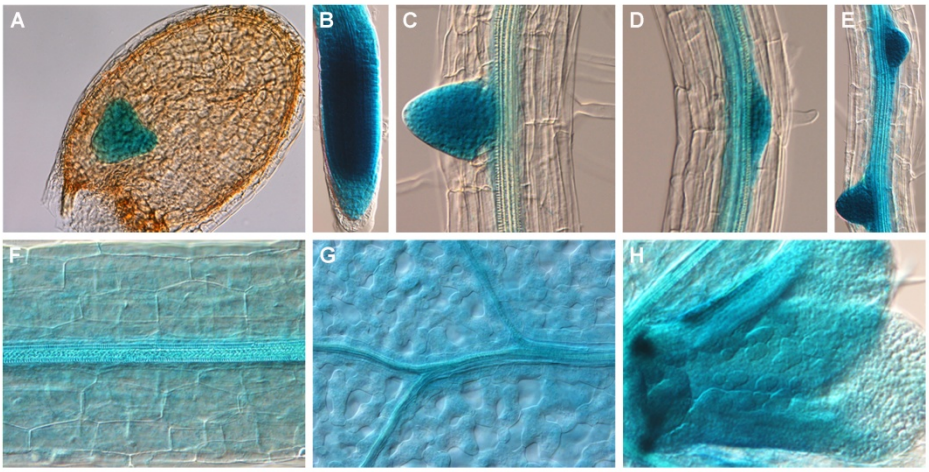

Supplemental Figure 6. *AP-3 β_{pro}:GFP-GUS* displays ubiquitous embryonic and postembryonic expression.

(A) to (H) GUS activity of *pAP-3 β::GFP-GUS* line is shown in the embryos (A) as well in 7-day-old seedlings ([B] to [H]). Note the higher expression of GUS in the meristematic zone of the primary root (B), emerging LR ([C] to [E]), upper part of the hypocotyl (F), as well in the cotyledons (G) and shoot apical meristem (H).

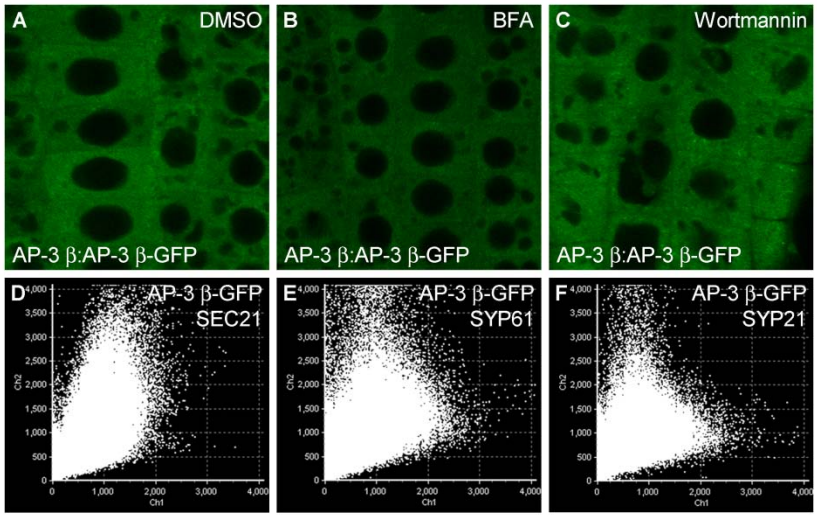

Supplemental Figure 7. AP-3 β-GFP localizes to a BFA- and wortmannin-insensitive compartment.

(A) to (C) AP-3 β-GFP localization in wild-type is shown after 2 h incubation in DMSO (A), 1 h of BFA (50 μM) (B) and 2 h of wortmannin (33 μM) (C) treatment.

(D) to (F) Degrees of colocalization of AP-3 β-GFP with SEC21 (Pearson's colocalization coefficient is 0.60332) (D), SYP61 (Pearson's coefficient is 0.59756) (E) and SYP21 (Pearson's coefficient is 0.55078) (F). Note that AP-3 β-GFP endosome-associated signal colocalizes only randomly with any of the tested markers. Colocalization degree was measured by the function of Olympus FV10 ASW software.

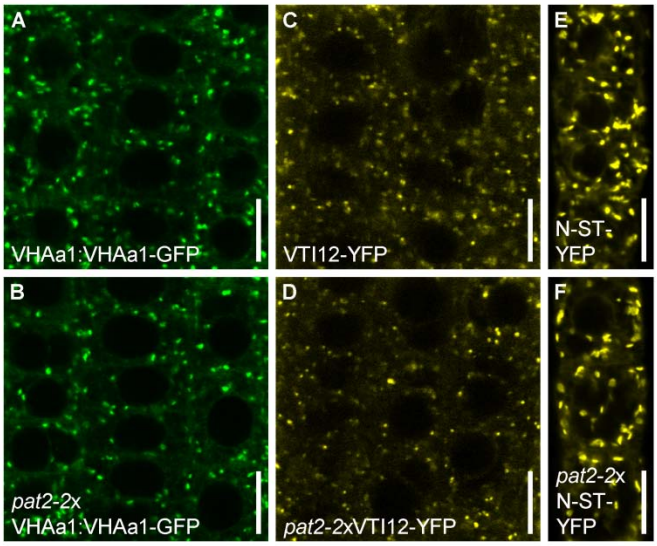

Supplemental Figure 8. *pat2* is not defective in the localization of Golgi and TGN markers.

(A) to (F) The localization of live imaged VHAa1-GFP, WAVE13/VTI12-YFP and N-ST-YFP is not obviously affected in *pat2-2* mutant ([B], [D] and [F]) as compared with the control ([A], [C] and [E]).

Scale bars are 10 μm.

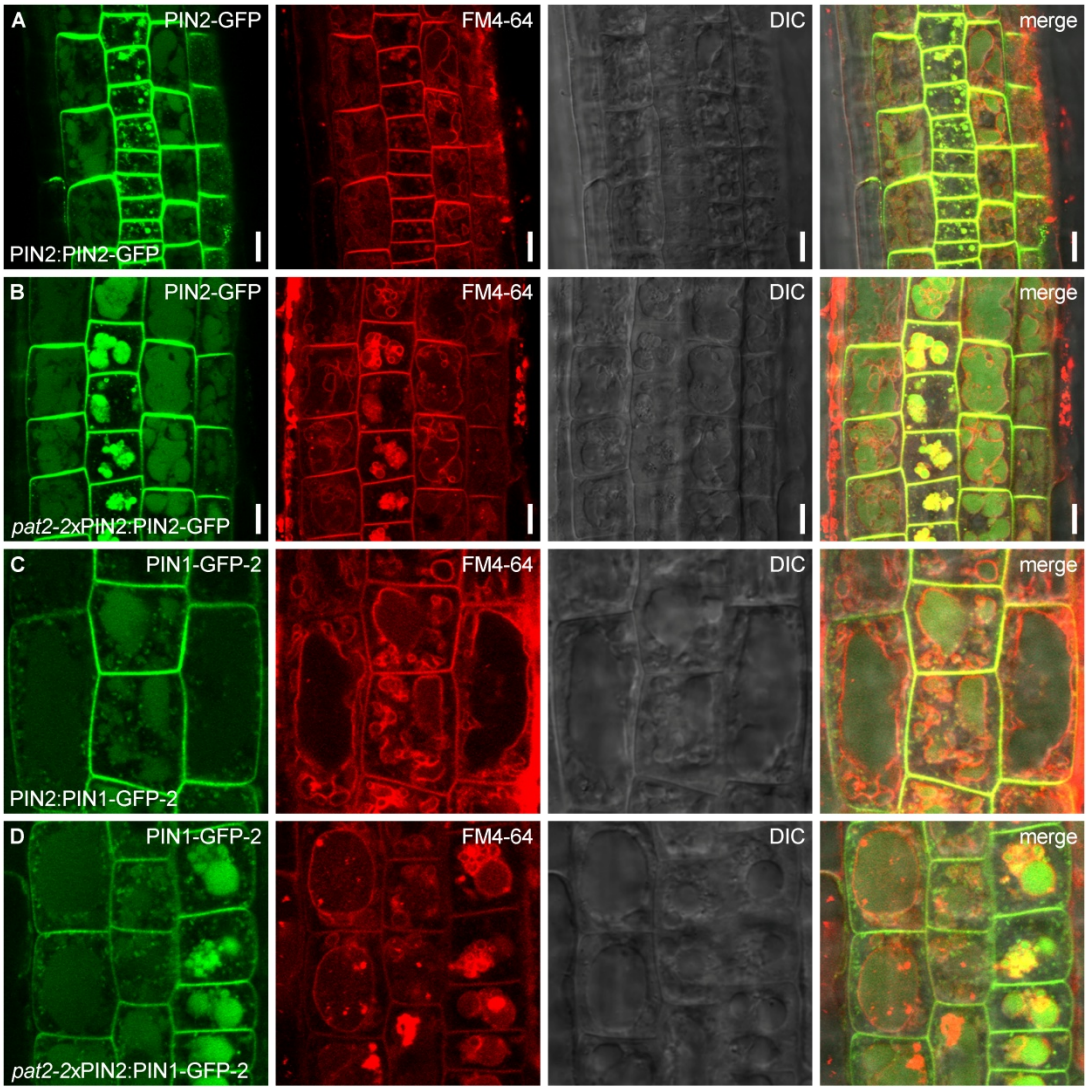

Supplemental Figure 9. *pat2* shows enhanced vacuolar accumulation of integral PM proteins and disrupted lytic vacuole morphology.

(A) to (D) Both, PIN2-GFP and PIN1-GFP-2 (green) shows enhanced accumulation in the *pat2-2* vacuoles following dark treatment (3 h) ([B] and [D]); Vacuoles were stained with FM4-64 (4 µM) (red). FM4-64 staining reveals stronger accumulation of PIN2-GFP and PIN1-GFP-2 in abnormal looking lytic vacuoles in *pat2-2* mutant ([B] and [D]) as compared to the control ([A] and [C]).

Scale bars are 10 µm.

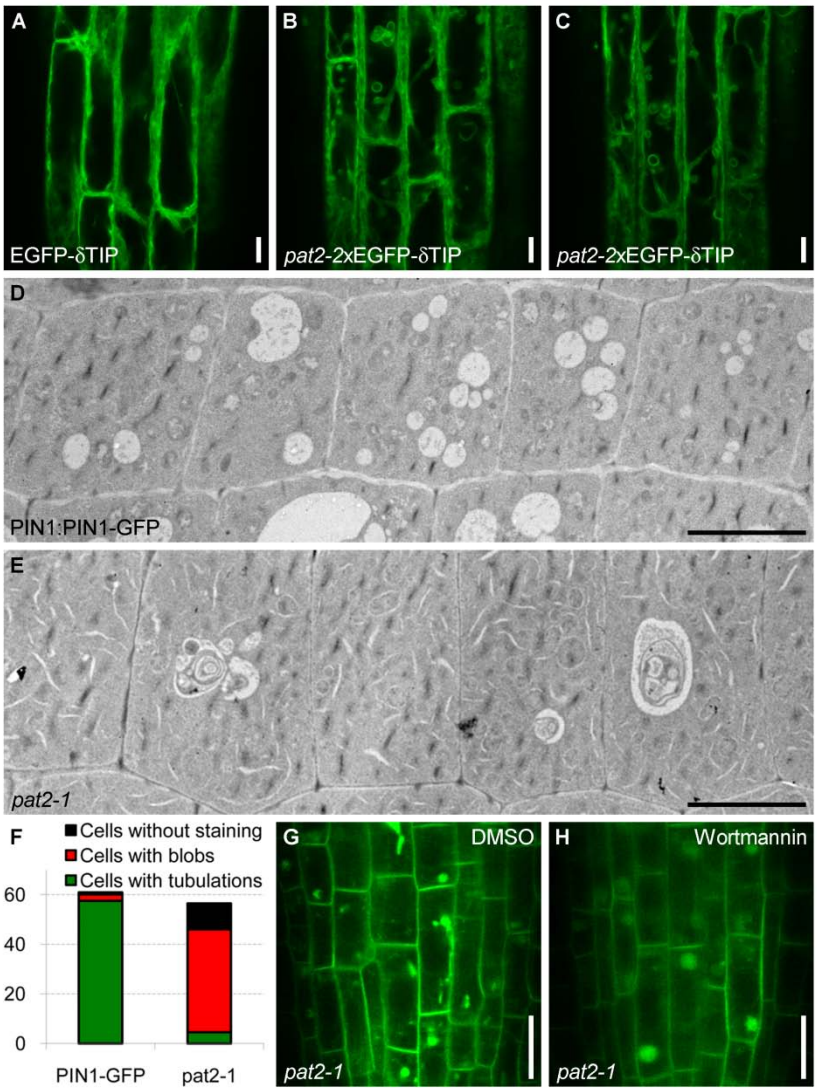

Supplemental Figure 10. *pat2* is defective in the morphology, biogenesis and identity of the lytic vacuole.

(A) to (C) Localization of GFP-δTIP in control (A) and *pat2-2* ([B] and [C]) reveals the existence of numerous bulb-like vacuolar structures in *pat2-2* epidermal cells.

(D) and (E) Electron micrographs showing the abnormal shape, size and number of *pat2-1* lytic vacuoles (E). Compare with the control (D).

(F) Quantification of BCECF (10 µM; 40 minutes) staining in cortex and endodermal cells of 5-day-old seedlings (n = 487 control cells; n = 452 *pat2-1* cells).

(G) and (H) PIN1-GFP accumulations in *pat2-1* mutant are sensitive to wortmannin. Compare *pat2-1* treated 1 h with DMSO (G) with *pat2-1*treated 1 h with wortmannin (33 µM; 1 h) (H).

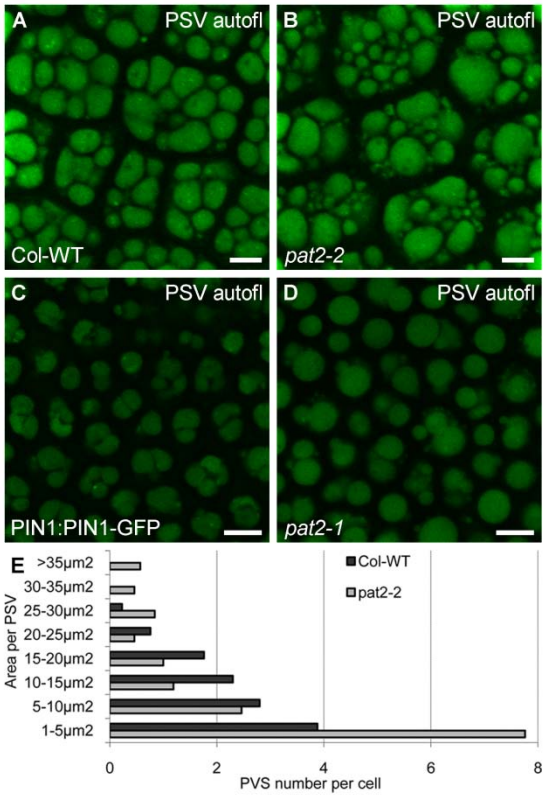

Supplemental Figure 11. *pat2* displays altered morphology of PSV.

(A) to (D) PSV autofluorescence (PSV autofl) (green) is shown in embryo root cells of wild type (A) and *pat2-2* (B) and embryo cotyledon cells of *PIN1*$_{pro}$*:PIN1-GFP* (C) and *pat2-1* (D). The images were collected after removing the coat of the seeds that were imbibed first for 1 h at 4^{o}C on a filter paper soaked with miliQ water.

(E) Histogram showing the PSV morphology of wild-type and *pat2-2* (n = 26).

Scale bars are 5 µm (A) and (B) and 10 µm (C) and (D).

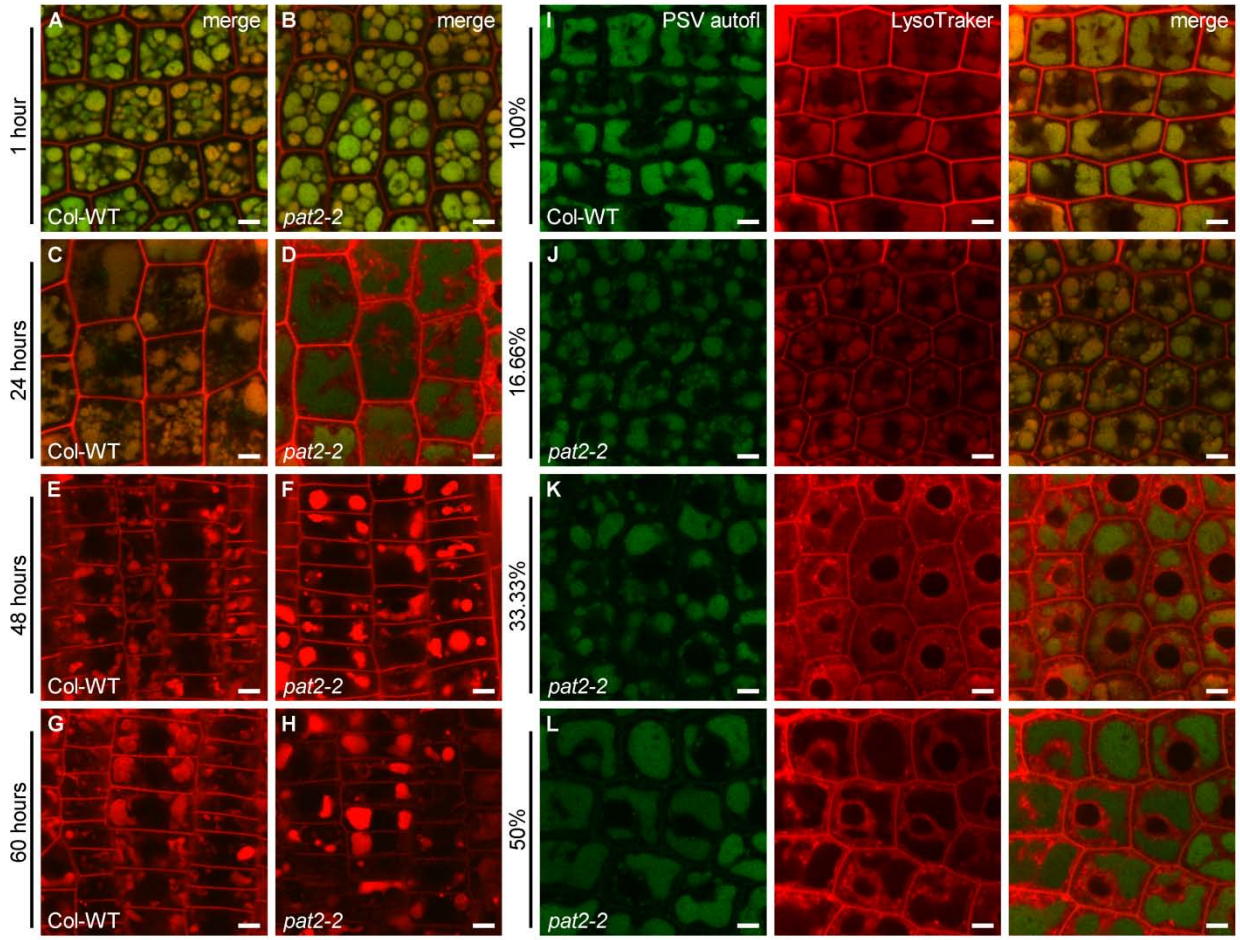

Supplemental Figure 12. *pat2* mutation disrupts the transition from PSVs to the lytic vacuoles**.**

(A) to (L) The development of PSVs (as shown by PSV autofluorescence; PSV autofl) within 60 h of growth on medium without sucrose and in continuous light (24^{o}C) is shown for wild-type ([A], [C], [E], [G] and [I]) and *pat2-2* ([B], [D], [F], [H] and [J] to [L]) embryo root cells. Images were collected 1 h after stratification ([A] and [B]), 18h later ([I] to [L]), 24 h later ([C] and [D]), 48 h later ([E] and [F]) and 60 h later ([G] and [H]) from embryos treated 1 h with LysoTracker red (2 µM; red). Note the impaired transition from PSV to the lytic vacuole in *pat2-2* as well as abnormal morphology of the *pat2-2* PSVs and lytic vacuoles. 18-h-old wild-type embryos show full colocalization of the PSV autofluorescence (green) with the pattern of LysoTracker red (2 µM) accumulation (red) (I). On the other hand, only 16.66% of *pat2-2* (J) embryos show full colocalization of the PSV autofluorescence with the LysoTracker red. 33.33% (K) and 50% (L) of *pat2-2* embryos show different accumulation pattern of the LysoTracker red showing that in the large proportion of *pat2* embryos the vacuole acidification during the transition from PSVs to lytic vacuoles is defective.

Scale bars are 5 μm.

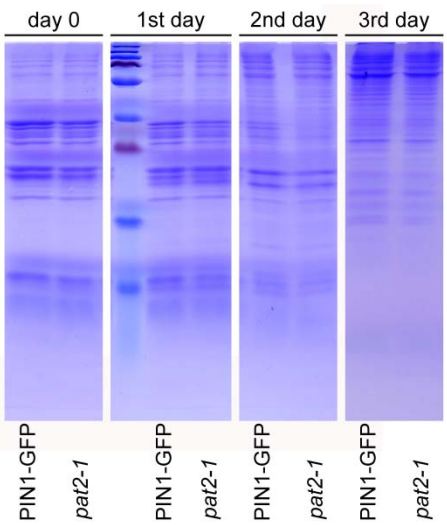

Supplemental Figure 13 *pat2* is not defective in the degradation of storage proteins.

SDS-PAGE on protein extract from germinating embryos: immediately after stratification (day 0), 1 day later, 2 days later and 3 days later.

SUPPLEMENTAL TABLES

Supplemental Table 1. List of *Arabidopsis* marker lines, crosses and constructs, and *S. cerevisiae* strains

No.	Line name	Accession number	Resistance	References
1	*pat2-1* (EMS mutant)	At3G55480	Kan for PIN1-GFP	This research
2	*pat2-2* (*β3* T-DNA mutant)	At3G55480/ N846552	PPT	This research; Alonso et al. (2003)
3	AP-3 β_{pro}:GUS-GFP in wild-type	At3G55480	Kan	This research
4	AP-3 β_{pro}:AP-3 β-GFP in *pat2-1*	At3G55480	PPT	This research
5	AP-3 β_{pro}:AP-3 β-GFP in WT	At3G55480	PPT	This research
6	$35S_{pro}$: AP-3 β-GFP in WT	At3G55480	Kan	This research
7	*pat2-2*xALE-GFP		PPT for SAIL *pat2-2*	This research
8	*pat2-2*xRABF1-GFP		PPT for SAIL *pat2-2*	This research
9	*pat2-2*xGFP-RABF2b		PPT for SAIL *pat2-2*	This research
10	*pat2-2*xδTIP-GFP		PPT for SAIL *pat2-2*	This research
11	*pat2-2*xN-ST-GFP		PPT for SAIL *pat2-2*	This research
12	*pat2-1*x*pat2-2*		PPT for SAIL *pat2-2*	This research
13	*pat2-2*xPIP2a-GFP		PPT for SAIL *pat2-2*	This research
14	*pat2-2*xSYP22-YFP		PPT for SAIL *pat2-2*	This research
15	*pat2-2*xVHAa1-GFP		PPT for SAIL *pat2-2*	This research
16	*pat2-2*xWAVE13Y/VTI12-YFP		PPT for SAIL *pat2-2*	This research
17	*pat2-2*xPIN2-GFP		PPT for SAIL *pat2-2*	This research
18	*pat2-2*xPIN1-GFP-2		PPT for SAIL *pat2-2*	This research
19	PIN1-GFPx*pat2-2*		PPT for SAIL *pat2-2*	This research
20	PIN7-GFPx*pat2-2*		PPT for SAIL *pat2-2*	This research
21	PIN2-GFPx *pat2-1*		PPT for SAIL *pat2-2*	This research
22	PIN1-GFP-2x*pat2-1*		PPT for SAIL *pat2-2*	This research
23	$35S_{pro}$:Aleurain-GFP	X05167		Di Sansebastiano et al. (2001)
24	$RABF1_{pro}$:RABF1-GFP	At3g54840		Jaillais et al. (2006)
25	$RABF2b_{pro}$:GFP-RABF2b	AT4g19640		Jaillais et al. (2006)
26	$35S_{pro}$:EGFP-δTIP	U39485		Cutler et al. (2000)
27	N-ST-YFP	AJ243198		Grebe et al. (2003)
28	$PIN1_{pro}$:PIN1-GFP	At1g73590		Benková et al. (2003)
29	$PIN2_{pro}$:PIN1-GFP-2	At1g73590		Wiśniewska et al. (2006)

30	$PIN2_{pro}$:PIN2-GFP	At5G57090		Xu et al. (2005)
31	$PIN7_{pro}$:PIN7-GFP	At1g23080		Blilou et al. (2005)
32	$35S_{pro}$:PIP2a-GFP	X75883		Cutler et al. (2000)
33	$SYP22_{pro}$:SYP22-YFP	U88045		Robert et al. (2008)
34	$VHAa1_{pro}$:VHAa1-GFP	At2g28520		Dettmer et al. (2006)
35	*vps29-3*	At3g47810		Kleine Vehn et al. (2008b)
36	WAVE13Y/VTI12-YFP	At1g26670		Geldner et al. (2009)
37	$AG425GPD_{pro}$:β3cDNA	At3g55480	SD-LEU	This research
38	pRS426:GFP-ALP		SD-URA	Cowles et al. (1997)
39	CCY255/*apl6Δ*	NP_011777		Cowles et al. (1997)
40	SEY6210/WT			Cowles et al. (1997)

Supplemental Table 2. List of primers

No.	Primer name	Sequence	Used for
1	β3SAIL_FP	CATCGGAAGTGAAGAAGCTTG	*pat2-2* genotyping
2	β3SAIL_RP	CCAGCTGCTGCTAGTACAACC	*pat2-2* genotyping
3	SAIL_LB3	TAGCATCTGAATTTCATAACCAATCTCGATACAC	*pat2-2* genotyping
4	attB1_β3_over/const_FP	GGGGACAAGTTTGTACAAAAAAGCAGGCTCGATGGCTGGGATTCGCTTACAT	Cloning: over expression of β3 genomic and constitutive expression of β3 cDNA for yeast complementation
5	attB2_β3_over/transl_RP	GGGGACCACTTTGTACAAGAAAGCTGGGTCAGTGGCTGAAGAAGACGGCTC	Cloning: over expression of β3 genomic (without stop) and translational fusion of β3 genomic (promoter plus gene without stop)
6	attB2_β3_const_RP	GGGGACCACTTTGTACAAGAAAGCTGGGTTTCAAGTGGCTGAAGAAGACGG	Cloning: constitutive expression of β3 cDNA for yeast complementation (plus stop)
7	attB1_β3_transl/transcr_FP	GGGGACAAGTTTGTACAAAAAAGCAGGCTCGGTTCCCTATAACTCTTTCTTA	Cloning: translational fusion of β3 genomic (native promoter and gene without stop) and promoter analysis
8	attB2_β3_transc_RP	GGGGACCACTTTGTACAAGAAAGCTGGGTCTGTACGAAGAGCCCAAGCCCT	Cloning: transcriptional fusion of β3 genomic (promoter analysis)
9	β3_RT_FP	ATGGCTGGGATTCGCTTACAT	RT-PCR
10	β3_RT_RP	GCGATAGATGAAGTGGTAGCA	RT-PCR
11	Tubulin_FP	ACTCGTTGGGAGGAGGAACT	RT-PCR
12	Tubulin_RP	ACACCAGACATAGTAGCAGAAATCAAG	RT-PCR

SUPPLEMENTAL METHODS

EMS mutagenesis, mutant forward genetics screen, and mapping

The mutants identified as displaying ectopic signal of PIN1-GFP in the stele cells and without obvious morphological phenotype under the standard growth conditions were designated as *pat* mutants. We mapped *pat2-1* to a region of 30 kb on the lower arm of chromosome 3 (20,559,605-20,589,205; BAC T22E16), with simple sequence length polymorphism (SSLP) and cleaved amplified polymorphic sequence (CAPS and dCAPS) markers. For the information about Col/L*er* polymorphism, we used the collection of SNPs and INDELs provided by Monsanto Arabidopsis Polymorphism and Ler Sequence Collection (Cereon Genomics) and TAIR (http://www.arabidopsis.org). The At3G55480 candidate gene was sequenced and a point mutation that caused a stop codon was found at the position 705 downstream of ATG.

Yeast constructs, transformation and complementation

Wild-type and *apl6Δ* yeast-competent cells were transformed with pRS426 GFP-ALP and selected for positives on SD-URA plates. Then, competent *apl6Δ* cells containing pRS426 GFP-ALP were transformed with *AG425GPD$_{pro}$:AP-3 β* and selected for positive transformants on SD-LEU-URA plates. The competent cells and the transformation were done with the Frozen-EZ Yeast Transformation II^{TM} Kit (Zymo Research) according to the manufacturer's instructions.

Quantitative analysis of hypocotyl gravitropic response

Plates with 2-day-stratified seeds were first illuminated for 6 h, then transferred to the dark. The seedlings were grown 48 h vertically, followed by 48 h of gravistimulation (90°). The plates were photographed and the collected images were used for the measurements. The hypocotyl gravitropic response of 75 seedlings from each line was measured by the angle function of Image J 1.41 software (http://rsbweb.nih.gov/ij/). The obtained values were processed with Excel 11.3.3 software (Microsoft Corporation) and converted to degrees of bending. For testing the shoot gravitropic response, 21-day-old plants were gravistimulated (90°) 90 min in the dark.

Quantitative analysis of emerged LRs

We counted the number of emerged LRs of 17-day-old seedlings grown on MS with and without sucrose (75 seedlings per each line). The arrested seedlings on MS without sucrose were excluded. The repetition gave more or less similar results, but depended much on the age of the mutant seeds used for the experiment.

Quantitative analysis of protein localization

For quantification of PIN1-GFP, the mean fluorescence intensity of the PIN1-GFP signal at the basal PM of stele cells was measured with Image J 1.41 software. To measure the fluorescence intensity, we used images of median sections of the meristematic zone. 10 stele cells per root and 11 roots per each line were analyzed. For quantification of aleurain-GFP localization, the fluorescence intensity of the aleurain-GFP signal along the cell files of the stele was measured on a distance of approximately 500 pixels. 3 files of stele cells were measured for each root and 12 roots were analyzed for each line. The individual values of all files were averaged and the obtained values were plotted.

Quantitative analysis of arrested seedlings

7-day-old seedlings grown on MS without sucrose were counted for both arrested and normal-looking phenotypes. For the quantitative analysis, we used 111 *PIN1*$_{pro}$*:PIN1-GFP*, 239 *pat2-2*, 181 wild-type, 210 *pat2-2* 2-month-old seeds and 247 *PIN1*$_{pro}$*:PIN1-GFP*, 167 *pat2-2*, 198 wild-type and 215 *pat2-2* 9-month-old seeds. The experiment was repeated several time and we could confirm the arrested phenotype of the mutant lines and the tightly correlation with the age of the seeds. For the complementation analysis, we counted 337 wild-type seedlings and 329 *AP-3* β_{pro}*:AP-3* β*-GFP* (in *pat2-1* background) 5-day-old seedlings.

FRAP analysis of PIN1-GFP

For the photobleaching experiment, 5-day-old *PIN1*$_{pro}$*:PIN1-GFP* (data not shown) and *pat2-1* seedlings were mounted in a chamber coverglass system (Lab-Tek®II) submerged with solid MS medium. A small region in the PM of a stele cell was selected for FRAP. The selected region was bleached by AR^{+} laser 488 nm of FV10-ASW Olympus confocal at laser full power for 100 sec. Images were collected before bleaching, immediately after bleaching, and within the recovery time.

RT-PCR

Total RNA was extracted from 2-week-old seedlings with the RNeasy Kit (Qiagen) according to the manufacturer's instructions. The cDNA was synthesized with the Superscript III reverse transcriptase kit (Invitrogen) according to the manufacturer's instructions. A transcript of 940 bp downstream of ATG was amplified. Primer sequences are listed in Supplemental Table 2.

Immunolocalization

Immunolocalization was done on seedlings 4-5 days after germination in an Intavis in situ pro robot according to the described protocol (Sauer et al., 2006). The primary antibodies used were used anti-PIN1 rabbit (Paciorek et al., 2005) 1:1000, anti-GFP rabbit (AbCam) 1:1000, anti-GFP mouse (Roche) 1:1000, anti-SYP61 rabbit (Sanderfoot et al., 2001) 1:500, anti-SYP21 rabbit (da Silva Conceiçao et al., 1997) 1:2000, anti-SEC21 rabbit (generously provided by D.G. Robinson) 1:800, and as the secondary antibodies Alexa488 anti-mouse (Invitrogen) 1:600, Alexa488 anti-rabbit (Invitrogen) 1:600, and Cy3 anti-mouse (Sigma) 1:600.

PSV microscopy and quantification

For quantification of PSV area, we measured the size of PSVs from 25 embryo cells per each line by the area function of Image J 1.41 software. The units of Image J were converted to μm^2 with an Objektmicrometer (474026-0000-000; Carl Zeiss 5+ $^{100}/_{100}$ mm). The obtained values were processed by Excel 11.3.3 software.

Most of the experiments were repeated 2-4 times and they gave similar results. For each independent experiment, 20 to 30 roots were analyzed and the most representative images are shown. The images were collected by Olympus FV10 ASW or Carl Zeiss CLSM confocal microscopes. Figures were processed and assembled in Photoshop CS4 (Adobe System).

SUPPLEMENTAL REFERENCES

Alonso, M., Stepanova, A.N., Leisse, T.J., Kim, C.J., Chen, H., Shinn, P., Stevenson, D.K., Zimmerman, J., Barajas, P., Cheuk, R., et al. (2003). Genome-wide insertional mutagenesis of *Arabidopsis thaliana*. Science **301:** 653-657.

da Silva Conceição, A.S., Marty-Mazars, D., Bassham, D.C., Sanderfoot, A.A., Marty, F., and Raikhel, N.V. (1997). The syntaxin homolog AtPEP12p resides on a late post-Golgi compartment in plants. Plant Cell **9:** 571–582.

Paciorek, T., Zazimalova, E., Ruthardt, N., Petrasek, J., Stierhof, Y.D., Kleine-Vehn, J., Morris, D.A., Emans, N., Jürgens, G., Geldner, N., et al. (2005). Auxin inhibits endocytosis and promotes its own efflux from cells. Nature **435:** 1251–1256.

Sanderfoot, A.A., Kovaleva, V., Bassham, D.C., and Raikhel, N.V. (2001). Interactions between syntaxins identify at least five SNARE complexes within the Golgi/prevacuolar system of the Arabidopsis cell. Mol. Biol. Cell **12:** 3733–3743.

Sauer, M., Paciorek, T., Benková, E., and Friml, J. (2006). Immunocytochemical techniques for whole-mount in situ protein localization in plants. Nat. Protocols **1:** 98-103.